The role of 14q32 microRNAs in vascular remodelling

Welten, S.M.J.

Chapter 4

Inhibition of MicroRNA-494 Reduces Carotid Artery Atherosclerotic Lesion Development and Increases Plaque Stability

Ann Surg 2015 Nov;262:841-848

A Wezel[1,2]
SMJ Welten[1,3]
W Razawy[1,2]
HM Lagraauw[2]
MR de Vries[1,3]
EAC Goossens[1,3]
MC Boonstra[1]
JF Hamming[1]
ER Kandimalla[4]
J Kuiper[2]
PHA Quax[1,3]
I Bot[1,2*]
AY Nossent[1,3*]

[*]Authors contributed equally to this work

[1]Department of Surgery, Leiden University Medical Center, Leiden, the Netherlands
[2]Division of Biopharmaceutics, LACDR, Leiden University, Leiden, the Netherlands
[3]Einthoven Laboratory for Experimental Vascular Medicine,
Leiden University Medical Center, Leiden, the Netherlands
[4]Idera Pharmaceuticals, Cambridge, MA, United States of America

Abstract

Objectives: Unstable atherosclerotic lesions in carotid arteries require surgical endarterectomy to reduce the risk of ischemic stroke. We aimed to identify microRNAs that exert a broad effect on atherosclerotic plaque formation and stability in the carotid artery.

Background: We made a selection of 164 genes involved in atherosclerosis. Using www.targetscan.org, we determined which microRNAs potentially regulate expression of these genes. We identified multiple microRNAs from the 14q32 microRNA cluster, which is highly involved in vascular remodeling. In human plaques, collected during carotid endarterectomy surgery, we found that 14q32 microRNA miR-494 was abundantly expressed in unstable lesions.

Methods: We induced atherosclerotic plaque formation in hypercholesterolemic ApoE$^{-/-}$ mice by placing semi-constrictive collars around both carotid arteries. We injected 'Gene Silencing Oligonucleotides' against miR-494 (GSO-494) or negative control (GSO-control). Using fluorescently labeled GSOs, we confirmed uptake of GSOs in affected areas of the carotids, but not elsewhere in the vasculature.

Results: After injection of GSO-494, we observed significant downregulation of miR-494 expression in the carotid arteries, while miR-494 target genes were upregulated. Further analyses revealed a 65% decrease in plaque size after GSO-494 treatment. Plaque stability was increased in GSO-494-treated mice, determined by an 80% decrease in necrotic core size and a 50% increase in plaque collagen content. Inhibition of miR-494 also resulted in decreased cholesterol levels and decreased VLDL fractions.

Conclusions: Treatment with GSO-494 results in smaller atherosclerotic lesions with increased plaque stability. Inhibition of miR-494 may decrease the risk of surgical complications or even avert endarterectomy surgery in some cases.

Introduction

Atherosclerosis in the carotid arteries is an important contributor to ischemic stroke. Carotid endarterectomy has proven to be effective in reducing the risk of ischemic stroke above carotid artery stenosis of 70%. Although patients with lower degrees of stenosis, between 50 and 69%, may also benefit from endarterectomy, the risk of surgical complications and per-operative Transient Ischemic Attack (TIA) or stroke currently appear to outweigh the benefits[1]. Besides atherosclerotic plaque size, plaque vulnerability is a major determinant of stroke risk[2,3]. Ideally, therapeutic strategies to decrease atherosclerotic disease would therefore not only address plaque size, but also plaque stability. Atherosclerosis is a complex, multifactorial disease in which various processes in immune modulation and cholesterol homeostasis are involved[4,5]. Taking into account this multifactorial nature of atherosclerosis, improvement of treatment strategies may be accomplished by targeting the process of atherogenesis as a whole rather than focusing on single factors.

MicroRNAs (miRs) are a class of short, non-coding RNAs, approximately 20 nucleotides long, capable of downregulating target gene expression at post-transcriptional level[6]. A single miR has, on average, 200 predicted target genes[7]. MiRs are excellent drug targets for complex diseases such as atherosclerosis, based on their ability to fine-tune expression of multiple genes[8,9]. Inhibition of miRs in atherosclerosis has been investigated in several studies and Rayner et al. showed that inhibiting miR-33 results in a lowering of plasma VLDL while increasing plasma HDL[10]. Besides regulation of cholesterol homeostasis, miRs have also been implicated in cellular mechanisms affecting atherosclerosis. MiR-126 for instance regulates post-transcriptional VCAM-1 expression in response to triglyceride-rich lipoproteins[11]. Also, inhibition of miR-92a has been demonstrated to up-regulate the expression of the atheroprotective Krüppel-like Factors KLF-2 and KLF-4 in endothelial cells[12,13]. Furthermore, smooth muscle cell proliferation and migration can be repressed by miR-195; consequently, neointima formation can be reduced by miR-195 gene therapy[14]. MiR-155 has been shown to repress the transcription factor Bcl6, thereby increasing NF-κB activation and CCL2 expression in macrophages[15]. However, it is apparent that most of these studies focus on the effect of miRs on a single cell type or process, thereby failing to do justice to the ability of miRs to exert a broad range of effects.

A commonly used tool to identify miRs involved in atherosclerosis is microarray profiling[16,17]. However, in order to utilize the specific characteristic of miRs to regulate many genes, we used a Reverse Target Prediction (RTP) strategy. Instead of investigating the miR with the highest regulation during atherosclerosis, we made use of a 'reversed' approach by taking multiple target genes as a starting point and subsequently selecting miRs that are predicted to regulate these genes. MiRs obtained by this method potentially target a larger subset of atherosclerosis-related genes and may thus function as a so-called 'master switch' in the development of atherosclerosis.

Using our unique RTP strategy, we identified miRs that are predicted to exert a broad effect on atherosclerosis. We singled out one miR from the large 14q32 miR-gene cluster, miR-494, which had thus far not been linked to atherosclerosis. Subsequently, we inhibited this miR using Gene Silencing Oligonucleotides (GSOs) in order to investigate its in vivo effect on atherosclerotic plaque formation and stability in the carotid artery.

Methods

A detailed description of the Materials and Methods is given in the Online Data Supplement.

Results

Identification of miRs From the 14q32 miR Gene Cluster by Reverse Target Prediction

We performed a RTP based on a list we compiled of atherosclerosis-related genes known from literature. As expected, we identified multiple miRs that have previously been described in atherosclerosis, including miR-155, miR-23/24,18 and miR-33. Interestingly, we found enrichment of binding sites for multiple miRs from a singe miR-gene cluster, located in an imprinted region on the long arm of human chromosome 14 (14q32; chromosome 12F1 in mice) (Supplemental Table 1A). We identified 11 miRs within this gene cluster, including miR-495 (45 putative targets), miR-494 (38 putative targets), and miR-329 (30 putative targets). We also performed our RTP by analyzing for murine target genes (Supplemental Table 1B), in which we again identified multiple targets for miR-495 (37 putative targets), miR-494 (34 putative targets), and miR-329 (26 putative targets). Recently, our group has shown an important role for miR-494, miR-495, and miR-329 in vascular remodeling[19] and we selected these miRs for further investigations.

Expression of miR-494, miR-495, and miR-329 in Human Atherosclerotic Plaques

To investigate whether miR-494, miR-495, and miR-329 are expressed in human atherosclerotic plaques, we isolated RNA from both stable and unstable lesions obtained from patients undergoing endarterectomy of the carotid artery. We detected abundant expression of miR-494 in all five unstable lesions and in one of three stable lesions. MiR-495 was expressed in all lesions, but at lower levels than miR-494, while the expression of miR-329 was not detectable in any of the lesions (Figure 1A).

Expression of miR-494, miR-495, and miR-329 in Murine Organs

In mouse carotid arteries, miR-494 and miR-495 are expressed approximately twice as high as miR-329 (Figure 1B). Analysis of the aorta revealed that the expression of miR-495 and miR-329 is higher as compared with miR-494. However, measurement of miR expression in the liver, spleen, bone marrow, and white blood cells demonstrated that the expression of miR-494 is higher as compared with miR-495 and miR-329 (Figure 1B). Taken into account the expression levels of miR-494 in murine organs and the higher expression of miR-494 in human atherosclerotic plaques, we selected miR-494 for further investigation regarding its effect on atherosclerotic lesion development.

In Vitro Target Gene Upregulation After Inhibition of miR-494

Inhibition of miR-494 led to a significant upregulation of the chemokine receptor CXCR4 in both endothelial cells and smooth muscle cells. Also, its ligand CXCL12 (SDF-1) was significantly increased in macrophages and mast cells. It has previously been shown that CXCR4/CXCL12 plays a protective role in atherosclerosis.[20,21] Inhibition of miR-494 also led to an upregulation of ACVR1 (a member of the TGF-beta superfamily) in macrophages and of TIMP3 (TIMP metallopeptidase inhibitor 3,

Supplemental Figure 1) in macrophages and mast cells.

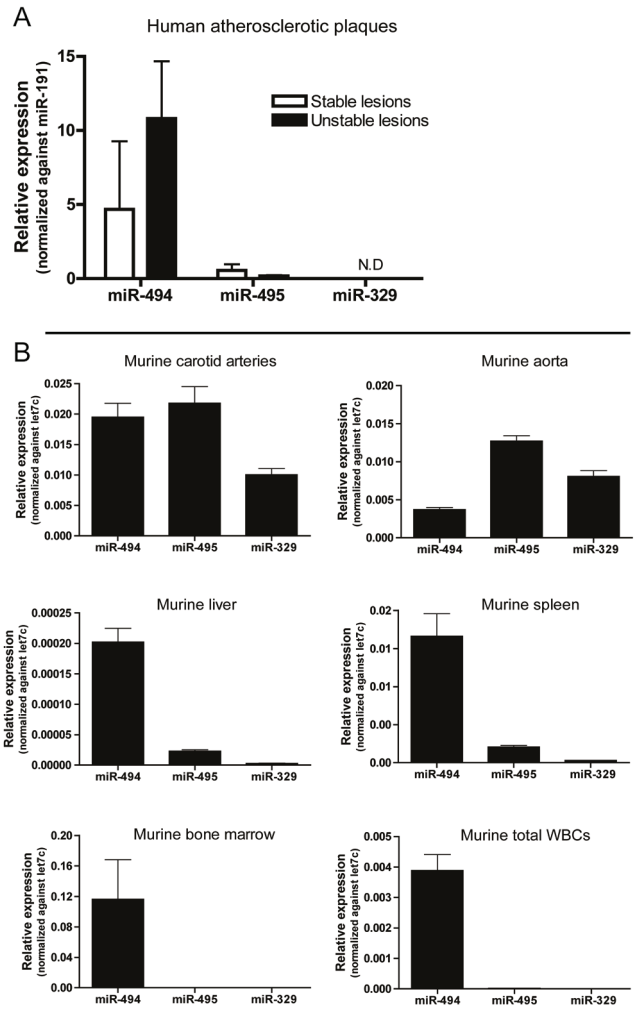

Figure 1. (A) Expression of miR-494, miR-495, and miR-329 in stable and unstable human carotid artery atherosclerotic plaques, relative to miR-191. (B) Expression of miR-494, miR-495, and miR-329, relative to miR-let-7c in the carotid artery, aorta, liver, spleen, bone marrow, and peripheral total white blood cells (WBCs) of ApoE$^{-/-}$ mice fed a western-type diet for three weeks.

Uptake of GSO-494 at Site of Collar Placement

At day 4 and 28, uptake of labeled GSO-494 (Figure 2) was clearly visible in the carotid artery in which the collar was placed, whereas no uptake was detected in the control carotid artery. Uptake of labeled GSO-494 was not observed in the aortic arch of mice fed a western-type diet for 2 weeks. However, a clear uptake of labeled GSO-494 was detected in the aortic arch of mice fed a western type diet for 6 weeks, which are known to contain early lesions. The descending aorta did not show any uptake of GSO-494. Also, no uptake was detected in the carotid arteries and aorta of control IRDye 800CW treated mouse.

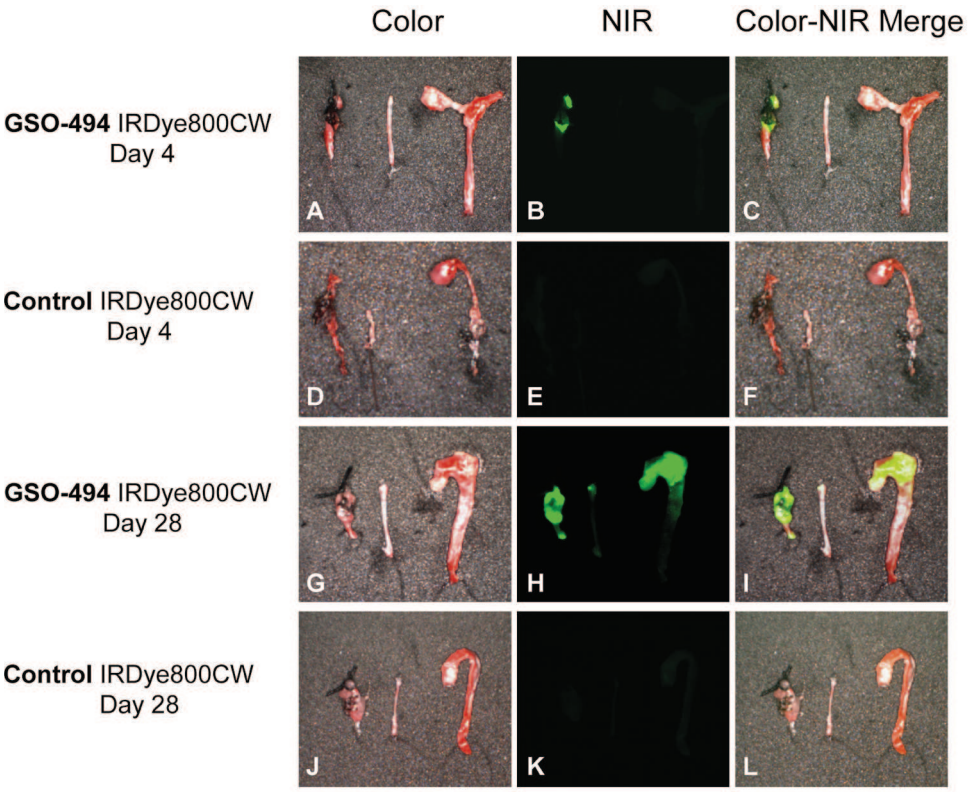

Figure 2. Uptake of IRDye 800CW-labeled GSO-494 or IRDye 800CW in the arterial wall. Each micrograph displays a carotid artery with collar induced atherosclerosis (left), contra-lateral control carotid artery from the same mouse without collar (middle), and aortic arch with descending aorta from the same mouse (left). Of note: all collars were removed before visualization. A-F: Arteries from mice receiving a high-cholesterol diet, 4 days after collar placement. (A) Arteries from mice 24 hours after intravenous injection of IRDye 800CW-labeled GSO-494. (B) Near-infrared (NR) image showing uptake of GSO-494 by the carotid artery in which a collar has been placed, which is absent in the control carotid artery. (C) Merged picture showing uptake of labeled GSO-494.
(D, E, F): Uptake of control unlabeled IRDye 800CW 24 hours after intravenous injection, 4 days after collar placement. G-L: Arteries from mice receiving a high-cholesterol diet, 28 days after collar placement, 24 hours after labeled GSO or control injection.
(G, H, I) Near-infrared (NR) image showing uptake of GSO-494 by the carotid artery in which a collar has been placed and in the aortic arch. No uptake is observed in the control carotid artery or in the descending aorta. (J, K, L) Uptake of control unlabeled IRDye 800CW 24 hours after intravenous injection, 4 weeks after collar placement.

In Vivo Repression of miR-494 and Target Gene Upregulation After GSO-494 Treatment

Three days after GSO-494 treatment, miR-494 was significantly downregulated by 46% in the carotid arteries compared with GSO-control (Figure 3A). Moreover, we observed upregulation of the selected target genes TIMP3, IL33, and TGFB2 in the carotid arteries of mice treated with GSO-494 (Figure 3B; $P < 0.05$).

Inhibition of miR-494 Affects Plasma Cholesterol Levels

Treatment with GSO-494 did not significantly affect either body weight (Supplemental Figure 2), or total white blood cell and cytokine levels (Supplemental Figure 3A and B). Also, body weight or plasma cholesterol levels did not differ between the PBS and GSO-control treated groups (Supplemental Figure 4A and B). Plasma cholesterol levels however showed a reduction of 13% after treatment with

GSO-494 (GSO-control: 30.4 ± 1.1 mM; GSO-494: 26.4 ± 0.7 mM; P < 0.01; Figure 4A). Lipid profiling using FPLC revealed that the reduced cholesterol level after inhibition of miR-494 was mainly owing to a decrease in the VLDL fraction (Figure 4B).

We aimed to elucidate the mechanism behind these changes in cholesterol levels by measurement of various target genes in liver and small intestine, which did not show any upregulation in gene expression after GSO-494 treatment (Supplemental Figure 5A and B). However, treatment of macrophages with GSO-494 in vitro resulted in a significant increase of cholesterol efflux towards HDL, compared with GSO-control treated cells (GSO-control: 8.1 ± 0.6% efflux; GSO-494: 10.4 ± 0.8%; P < 0.05; Figure 4C).

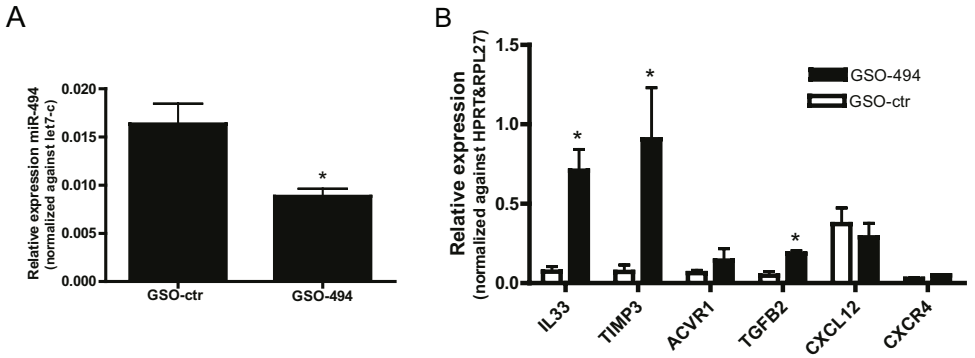

Figure 3. (A) Expression of miR-494 in carotid arteries of ApoE-/- mice, 4 days after injection of either GSO-494 or GSO-control (GSO-ctr), relative to expression of miR-let-7c. (B) Expression of selected target genes IL-33, TIMP3, ACVR1, TGFB2, CXCL12, and CXCR4 in carotid arteries of ApoE-/- mice, 4 days after injection of either GSO-494 or GSO-ctr, relative to expression of HPRT & RPL27.
*P < 0.05 compared with GSO-ctr.

Inhibition of miR-494 Reduces Atherosclerotic Lesion Formation

Atherosclerotic plaques were analyzed for size and composition and interestingly, revealed a marked reduction of 65% in atherosclerotic plaque size in the group treated with GSO-494 (GSO-control: 47 ± 11×103 μm^2; GSO-494: 16 ± 3×103 μm^2; P < 0.05; Figure 4D). We did not observe differences in lesion size between PBS and GSO-control treated groups (Supplemental Figure 4C), illustrating that GSOs did not exert nonspecific effects.

Treatment With GSO-494 Leads to an Enhanced Stable Phenotype of Atherosclerotic Lesions

Atherosclerotic plaques were not only reduced in size after treatment with GSO-494; the plaques also showed an increase in plaque stability. So-called “stable lesions” are characterized by a small necrotic core and a thick fibrous cap rich in collagen and smooth muscle cells. Indeed, necrotic core size was significantly reduced by 80% in mice treated with GSO-494 (GSO-control: 33 ± 6%; GSO-494: 6 ± 3%; P < 0.001; Figure 5A). Furthermore, collagen content was significantly increased after inhibition of miR-494 (GSO-control: 6.6 ± 1.6%; GSO-494: 12.7 ± 2.1%; P < 0.05; Figure 5B).

Plaque morphology was further examined by visualizing smooth muscle cells using an alpha smooth muscle actin staining. The percentage of positively stained lesion area was similar in both treatment groups (GSO-control: 4.6 ± 1.0%; GSO-494: 6.4 ± 1.8%; Figure 5C); moreover, lesional macrophage content remained unaltered after GSO-494 treatment (GSO-control: 20.0 ± 2.2%; GSO-494: 23.6 ± 2.7%; Figure 5D). We also stained for mast cells, as these have previously been described as important

players in atherosclerotic plaque development and destabilization.[22,23] However, no differences were found in either mast cell numbers (Figure 5E) or in their activation status (data not shown).

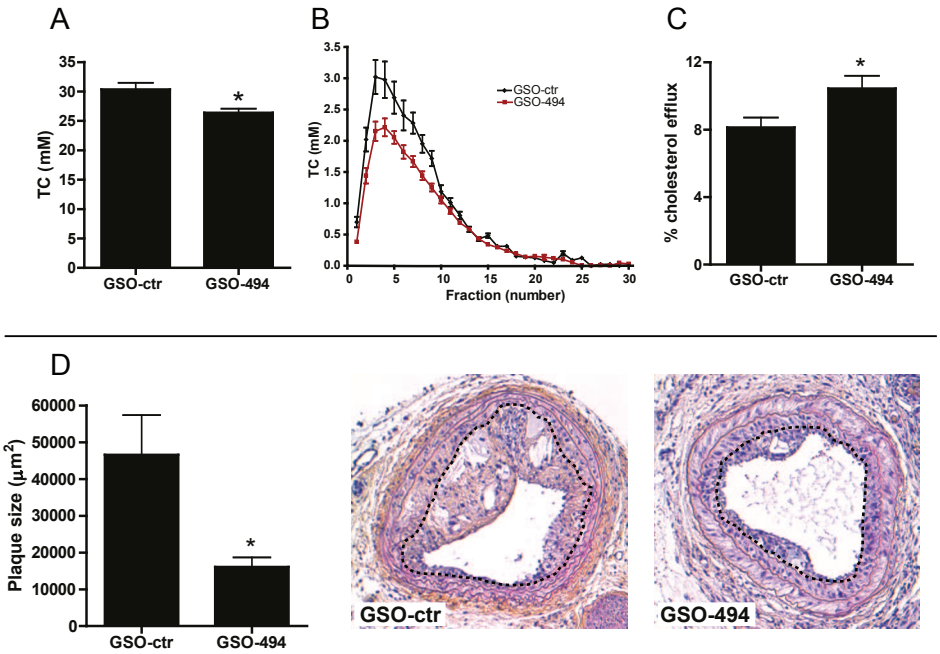

Figure 4. (A) Total plasma cholesterol levels of ApoE$^{-/-}$ mice treated with GSO-494 compared with GSO-control (GSO-ctr), 6 weeks after start of the western-type diet. (B) AKTA-FPLC analysis revealed a decrease in VLDL/LDL levels in mice treated with GSO-494 compared with GSO-ctr. (C) Cholesterol efflux towards HDL in macrophages treated with GSO-494 or GSO-ctr in vitro. (D) Maximal plaque size (µm2) in carotid arteries of ApoE$^{-/-}$ mice treated with GSO-494 compared with GSO-ctr. Micrographs show representative images of both treatment groups (100x enlarged). *P < 0.05, compared with GSO-ctr.

Inhibition of miR-494 Results in Altered Collagen Homeostasis

To elucidate the mechanism behind the increased amount of collagen present in the plaque, we studied both collagen synthesis and collagen degradation in an in vitro setup. Inhibition of miR-494 in smooth muscle cells did not result in increased collagen synthesis rate (Supplemental Figure 6A). Regarding collagen degradation, we determined TIMP expression after treatment of cultured cells with GSO-494, as TIMPs inhibit matrix degradation by MMPs. TIMP3 is a predicted target of miR-494 and indeed, the expression levels of TIMP3 were increased in mast cells (1.5-fold; P < 0.05) and macrophages (21-fold; P < 0.05) after inhibition of miR-494. The expression levels of MMP9 remained unchanged after treatment with GSO-494, resulting in a net increase in TIMP/MMP ratio (Supplemental Figure 6B).

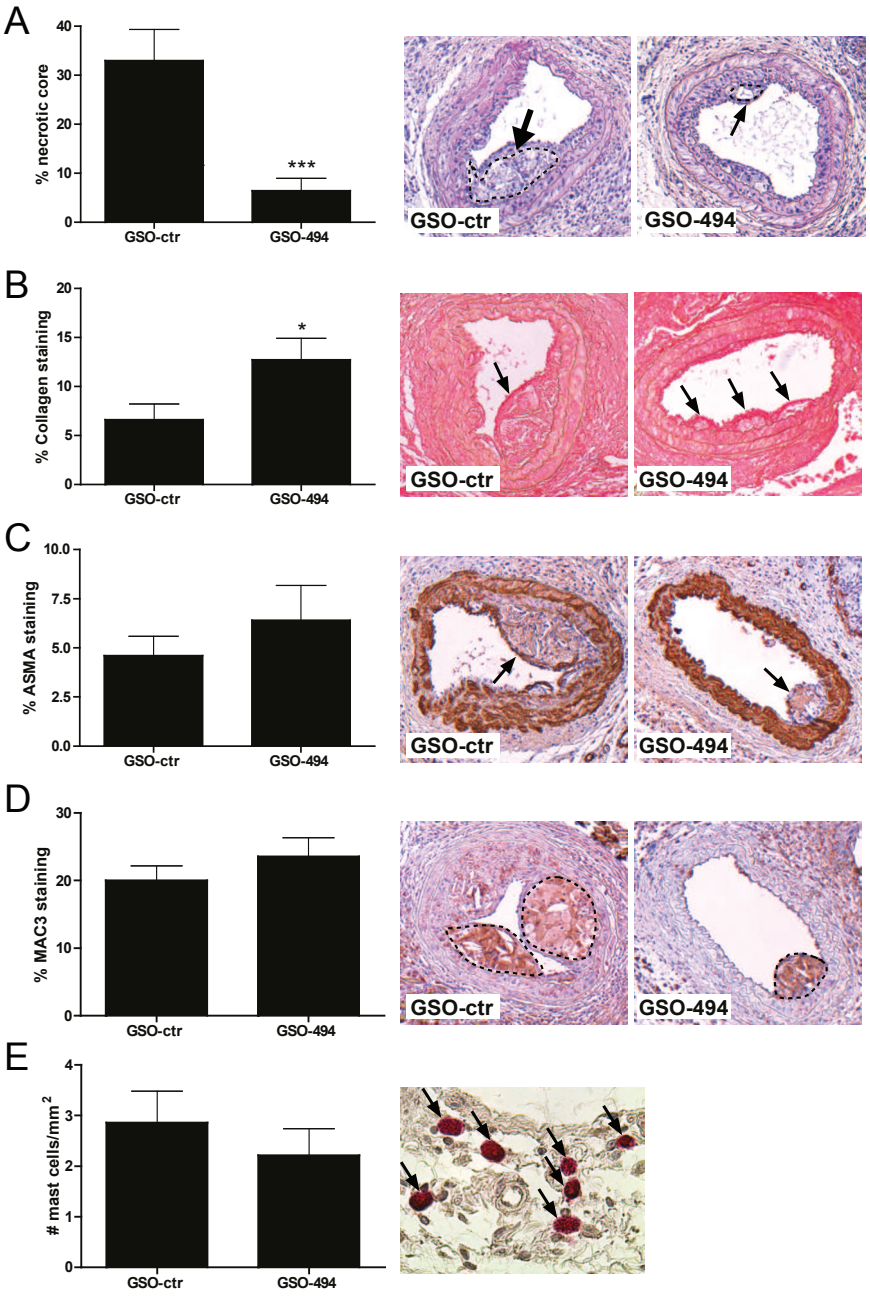

Figure 5. Effect of miR-494 inhibition on plaque morphology and lesion stability. (A) Necrotic core size was defined as an acellular area rich of debris and was measured as a percentage of total plaque area. Necrotic cores are indicated by dashed lines and arrows. (B) Collagen content in the lesions of mice treated with either GSO-494 or GSO-control (GSO-ctr). Collagen-positive areas are indicated by arrows. (C) Smooth muscle cells in the plaque were stained with an antibody against [alpha]-SMA (indicated by arrows), whereas (D) macrophages were visualized with a MAC-3 antibody (dashed lines). (E) Resting mast cells in the perivascular tissue of mice treated with either GSO-494 or GSO-ctr are indicated by arrows. The micrographs show representative images of both groups (A-D: 100x; E: 400x). *P < 0.05, ***P < 0.001, compared with GSO-ctr.

Discussion

The current study is the first to report a role for miR-494 from the 14q32 miR-gene cluster in the development of atherosclerosis. We used a unique RTP strategy to identify miR-494, by combining knowledge from our own previous experiments and literature in an in silico approach. Besides recovering miRs known to be important in atherosclerosis, we identified miRs that had not yet been investigated in this disease, in particular miRs from the 14q32 cluster. The 14q32 miR gene cluster is highly conserved in mammals and consists of 61 miR genes in mice and 54 in human[24]. Previously, it has been shown that many of the 14q32 miRs are implicated in human disease[25]. A recent study by Aavik et al[26] showed that hypomethylation of the 14q32 locus is associated with atherosclerosis. We showed that 14q32 miR-494 is abundantly expressed in human atherosclerotic plaques, in particular in unstable lesions. Also, miR-494 was found to be expressed in the murine carotid artery wall, and in other organs involved in the development of atherosclerosis, such as the liver and the spleen. In vivo, inhibition of miR-494 resulted in a decrease in atherosclerotic plaque formation with a marked increase in plaque stability.

Even though miR-494 was predicted to target more pro- than anti-inflammatory target genes in our RTP, the in vivo effects of inhibiting miR-494 revealed a positive effect on atherosclerosis. This may be explained by the fact that several atheroprotective genes, including TGFB2[27] or IL33[28] were upregulated in vivo after GSO-494 treatment. Numerous studies have targeted proatherogenic genes to reduce atherosclerosis, but our data suggest that upregulation of antiatherogenic genes may be just as, or even more, promising when treating this complex disease.

In our study, we inhibited miR-494 by means of GSOs, as described previously[19]. We were able to detect fluorescently labeled GSO-494 in the affected area of the carotid artery in which collars were placed, but not in control carotids. Moreover, uptake of labeled GSO-494 was observed in the aortic arch, which is known to contain lesions in $ApoE^{-/-}$ mice fed a western-type diet for 6 weeks. These data show that GSOs are targeted to atherosclerotic lesions. This is highly relevant for therapeutic applicability of GSOs, as patients at risk of atherosclerotic complications, such as TIA and/or stroke, already have advanced atherosclerotic lesions.

Inhibition of miR-494 reduced plasma cholesterol levels by 13%. Surprisingly, we did not detect any regulation of miR-494 target genes related to lipid or cholesterol metabolism in the liver. Also, target gene expression in the intestine of GSO treated mice was unaltered. We did however observe a significant increase in HDL-mediated efflux in vitro in macrophages treated with GSO-494 compared with GSO-control. This suggests that inhibition of miR-494 increases the removal of excess cholesterol from the vessel wall to the liver via HDL, resulting in reduced atherogenesis and a reduced necrotic core size in the lesions.

Besides the reduction in necrotic core size, plaque stability under miR-494 inhibition was further increased by an increase in collagen content. We initially hypothesized that this may have been caused by increased collagen homeostasis. However, no changes in collagen synthesis rate were detected after treating smooth muscle cells in vitro with GSO-494. The TIMP/MMP ratio was significantly increased however, indicative of decreased collagen degradation. In vivo, decreased collagen degradation results in an increased thickness of the fibrous cap, thereby reducing the risk of plaque rupture with concomitant cardiovascular events, including TIA and/or stroke.

Involvement of miR-494 in atherosclerosis had not previously been shown. However, our group has recently described a role of miR-494 in therapeutic neovascularization. For patients suffering from ischemia, restoring blood flow to the downstream tissues is crucial. Stimulating arterio- and angiogenesis, however, is always accompanied by an inflammatory reaction, which often leads to an aggravation of the underlying cause of the ischemia: atherosclerosis. This so-called Janus phenomenon[29] is a major drawback in this field of research, especially when translating controlled, univariate animal models towards a clinical setting. Intriguingly, our group showed that inhibition of miR-494 leads to a profound increase in blood flow after hindlimb ischemia[19]. Therapeutic inhibition of miR-494 may therefore be unique in inducing neovascularization, whereas simultaneously reducing atherosclerosis formation and increasing plaque stability in patients with occlusive arterial disease.

In conclusion, we discovered a role for miR-494 from the 14q32 miR gene cluster in atherosclerosis by utilizing the specific characteristic of miRs to regulate multiple genes and cellular processes. Inhibition of miR-494 led to a reduction in lesion size and an increase in plaque stability in mice. As miR-494 expression was also elevated in unstable human atherosclerotic plaques, future studies will have to determine whether our findings in this murine model also apply in a clinical setting. As both carotid artery plaque size and stability are major determinants of risk of TIA and/or stroke, this would make miR-494 a promising new therapeutic target for patients suffering from carotid artery atherosclerosis as well as for other occlusive arterial diseases.

Acknowledgments
The authors would like to thank Dr. JFP Berbée and Dr. GHM van Puijvelde for their technical support, the Netherlands Organization for Scientific Research (NWO; Veni 916.12.041), the Leiden University Fund/Nypels-van der Zee Fund (2219/5-4-12\NZ), and the Netherlands Institute for Regenerative Medicine (NIRM; FES0908).

References

1. Rothwell PM, Eliasziw M, Gutnikov SA, et al.; Carotid Endarterectomy Trialists' Collaboration. Analysis of pooled data from the randomised controlled trials of endarterectomy for symptomatic carotid stenosis. *Lancet*. 2003;361:107-116.
2. Shah PK. Mechanisms of plaque vulnerability and rupture. *J Am Coll Cardiol*. 2003;41:15S-22S.
3. Saba L, Potters F, van der Lugt A, et al. Imaging of the fibrous cap in atherosclerotic carotid plaque. *Cardiovasc Intervent Radiol*. 2010;33:681-689.
4. Galkina E, Ley K. Immune and inflammatory mechanisms of atherosclerosis. *Annu Rev Immunol*. 2009;27:165-197.
5. Libby P. Inflammation in atherosclerosis. *Arterioscler Thromb Vasc Biol*. 2012;32:2045-2051.
6. Chen K, Rajewsky N. The evolution of gene regulation by transcription factors and microRNAs. *Nat Rev Genet*. 2007;8:93-103.
7. Rajewsky N. MicroRNA target predictions in animals. *Nat Genet*. 2006;38:S8-S13.
8. van Rooij E, Olson EN. MicroRNA therapeutics for cardiovascular disease: opportunities and obstacles. *Nat Rev Drug Discov*. 2012;11:860-872.
9. Nossent AY, Eskildsen TV, Andersen LB, et al. The 14q32 MicroRNA-487b Targets the Antiapoptotic Insulin Receptor Substrate 1 in Hypertension-Induced Remodeling of the Aorta. *Ann Surg*. 2013;258:743-753.
10. Rayner KJ, Esau CC, Hussain FN, et al. Inhibition of miR-33a/b in non-human primates raises plasma HDL and lowers VLDL triglycerides. *Nature*. 2011;478:404-407.
11. Sun C, Alkhoury K, Wang YI, et al. IRF-1 and miRNA126 modulate VCAM-1 expression in response to a high-fat meal. *Circ Res*. 2012;111:1054-1064.
12. Fang Y, Davies PF. Site-specific microRNA-92a regulation of Kruppel-like factors 4 and 2 in atherosusceptible endothelium. *Arterioscler Thromb Vasc Biol*. 2012;32:979-987.
13. Alaiti MA, Orasanu G, Tugal D, et al. Kruppel-like factors and vascular inflammation: implications for atherosclerosis. *Curr Atheroscler Rep*. 2012;14:438-449.
14. Wang YS, Wang HY, Liao YC, et al. MicroRNA-195 regulates vascular smooth muscle cell phenotype and prevents neointimal formation. *Cardiovasc Res*. 2012:95:517-526.
15. Nazari-Jahantigh M, Wei Y, Noels H, et al. MicroRNA-155 promotes atherosclerosis by repressing Bcl6 in macrophages. *J Clin Invest*. 2012;122:4190-4202.
16. Zhu J, Chen T, Yang L, et al. Regulation of microRNA-155 in atherosclerotic inflammatory responses by targeting MAP3K10. *PLoS One*. 2012;7:e46551.
17. J i R, Cheng Y, Yue J, et al. MicroRNA expression signature and antisense-mediated depletion reveal an essential role of MicroRNA in vascular neointimal lesion formation. *Circ Res*. 2007;100:1579-1588.
18. Boon RA, Hergenreider E, Dimmeler S. Atheroprotective mechanisms of shear stress-regulated microRNAs. *Thromb Haemost*. 2012;108:616-620.
19. Welten SM, Bastiaansen AJ, de Jong R, et al. Inhibition of 14q32 MicroRNAs miR-329, miR-487b, miR-494 and miR-495 Increases Neovascularization and Blood Flow Recovery after Ischemia. *Circ Res*. 2014;115:696-708.
20. Zernecke A, Bot I, Djalali-Talab Y, et al. Protective role of CXC receptor 4/CXC ligand 12 unveils the importance of neutrophils in atherosclerosis. *Circ Res*. 2008;102:209-217.
21. Bot I, Daissormont IT, Zernecke A, et al. CXCR4 blockade induces atherosclerosis by affecting neutrophil function. *J Mol Cell Cardiol*. 2014;74C:44-52.
22. Bot I, de Jager SC, Zernecke A, et al. Perivascular mast cells promote atherogenesis and induce plaque destabilization in apolipoprotein E-deficient mice. *Circulation*. 2007;115:2516-2525.
23. Willems S, Vink A, Bot I, et al. Mast cells in human carotid atherosclerotic plaques are associated with intraplaque microvessel density and the occurrence of future cardiovascular events. *Eur Heart J*. 2013;34:3699-3706.
24. Seitz H, Royo H, Bortolin ML, et al. A large imprinted microRNA gene cluster at the mouse Dlk1-Gtl2 domain. *Genome Res*. 2004;14:1741-1748.
25. Benetatos L, Hatzimichael E, Londin E, et al. The microRNAs within the DLK1-DIO3 genomic region: involvement in disease pathogenesis. *Cell Mol Life Sci*. 2013;70:795-814.
26. Aavik E, Lumivuori H, Leppänen O, et al. Global DNA methylation analysis of human atherosclerotic plaques reveals extensive genomic hypomethylation and reactivation at imprinted locus 14q32 involving induction of a miRNA cluster. *Eur Heart J*. 2015;36(16):993-1000.
27. Mallat Z, Gojova A, Marchiol-Fournigault C, et al. Inhibition of transforming growth factor-beta signaling accelerates atherosclerosis and induces an unstable plaque phenotype in mice. *Circ Res*. 2001 ;89:930-934.
28. Pei C, Barbour M, Fairlie-Clarke KJ, et al. Emerging role of interleukin-33 in autoimmune diseases. *Immunology*. 2014;141:9-17.
29. Epstein SE, Stabile E, Kinnaird T, et al. Janus phenomenon: the interrelated tradeoffs inherent in therapies designed to enhance collateral formation and those designed to inhibit atherogenesis. *Circulation*. 2004;109:2826-2831.

Supplemental Material

Materials and Methods

Reverse Target Prediction
Based on existing knowledge from both literature[1-5] and previous studies within our group, we compiled a list of 164 genes involved in atherosclerosis. Using the online algorithm Targetscan (www.targetscan.org), a list was generated of all miRs predicted to target our selected genes. We ranked the miRs according to the number of putative target genes with a predicted 3'UTR binding site. The RTP was performed by analyzing binding sites in human target genes to ensure clinical relevance (Supplemental table 1A). We then performed the RTP by analyzing binding sites in murine target genes, to confirm the validity of the use of our mouse model for atherosclerosis (Supplemental table 1B).

Human carotid artery plaques
Human were collected anonymously during endarterectomy surgery at the Leiden University Medical Center. Plaques were fixed in 4% formaldehyde and embedded in paraffin. From a biobank of approximately 50 human carotid artery plaques, 6 highly unstable and 6 relatively stable plaques were selected based on three parameters for plaque instability (i.e. necrotic core size, macrophage content and intra-plaque hemorrhage). Total RNA was isolated using the RNeasy FFPE Kit according to manufacturer's protocol (Qiagen). Sufficient RNA was isolated from 3 stable and 5 unstable plaques for miR quantification as described below.
According to Dutch law, no informed consent is required for the collection human tissue samples, as long as only fully anonymized 'leftover' material is collected and stored.

Mice
All animal work was performed in compliance with the Dutch government guidelines and the Directive 2010/63/EU of the European Parliament. Male ApoE$^{-/-}$ mice, obtained from the local animal breeding facility (Gorlaeus Laboratories, Leiden University, Leiden, the Netherlands), were fed a Western type diet, containing 0.25% cholesterol and 15% cacao butter (SDS, Sussex, UK) for six weeks. Before surgical intervention mice were age-, cholesterol-, and weight-matched. Details of cholesterol measurement are described below. White blood cell (WBC) numbers and cellular differentiation were determined on a Sysmex cell differentiation apparatus (Goffin Meyvis, Etten-Leur, The Netherlands).

Carotid collar placement
Two weeks after start of the Western type diet, carotid artery plaque formation was induced by perivascular collar placement as described previously[6]. Before surgery and sacrifice, mice were anaesthetized by an intra-peritoneal injection with midazolam (5 mg/kg; Roche, Woerden, The Netherlands), domitor (0.5 mg/kg; AST Farma, Oudewater, The Netherlands) and fentanyl (0.05 mg/kg; Janssen, Beerse, Belgium). After surgery, mice were antagonized with a subcutaneous injection of flumazenil (0.5 mg/kg; Fresenius Kabi, Schelle, Belgium), antesedan (2.5 mg/kg; AST Farma) and buprenorphine (0.1 mg/kg; MSD Animal Health, Boxmeer, The Netherlands). In brief, a semi-constrictive collar was placed around both left and right carotid arteries of the mice. Low shear stress and disturbed flow at the proximal site of the collar result in increased expression of endothelial adhesion molecules and atherosclerotic lesion formation. At either one week or four weeks after collar placement, mice were anaesthetized and in situ perfused, after which carotid artery lesions were harvested for further analysis.

Treatment with IRDye labelled GSOs
Four male adult ApoE$^{-/-}$ mice received one perivascular collar around the right carotid artery, while the contra-lateral carotid artery was left unaffected. At day 4 and day 28 after surgery, mice were injected intravenously with IRDye-800CW-labelled GSO-494 (0.4mg/mouse; Idera Pharmaceuticals, Cambridge MA) or control unlabelled IRDye. Mice were sacrificed by orbital exsanguination one day after injection. Near-InfraRed (NIR) fluorescence measurements were performed using the FLARE™ NIR imaging system7.

Treatment with GSOs
At day 4 after surgery, mice received an intravenous injection of either 1 mg Gene Silencing Oligonucleotide dissolved in 200 µl PBS (GSO, kindly provided by Idera Pharmaceuticals, Cambridge, MA, USA) or 200 µl PBS control at day 4 after surgery. A subset of mice (n=6 per group) was sacrificed 3 days later (1 week after surgery) in order to establish downregulation of miR-494 in vivo. For effects on atherosclerosis, the remaining mice received a second injection of 0.5 mg GSO dissolved in 200 µl PBS per mouse at day 18 (n=15 per group). GSO-494 was designed with perfect reverse complementarity to the mature target miR sequence and synthesized by Idera Pharmaceuticals. As a negative control, a scrambled sequence was used, designed not to target any known murine miR. GSOs consist of two single-stranded O-methyl-modified DNA strands, linked together at their 5'ends by a phosphorothioate-linker to avoid TLR-activation[8,9]. Sequences of GSOs used are given in Supplemental table 2.

Plasma analysis
Blood was collected from the mice by tail bleeding. The concentration of cholesterol in plasma was determined by incubation with 0.025 U/ml cholesterol oxidase (Sigma, Zwijndrecht, The Netherlands) and 0.065 U/ml peroxidase and 15 µg/mL cholesterol esterase (Roche Diagnostics, Mannheim, Germany) in polyoxyethylene-9-laurylether, and 7.5% methanol). Precipath (standardized serum; Boehringer Mannheim, Germany) was used as an internal standard. Absorbance was measured at 490 nm.

For lipid profiling, plasma was pooled (n=3 mice per sample) and diluted 6 times, after which fractionation of plasma lipoproteins was performed using an AKTA-FPLC. Triglyceride levels and total cholesterol levels were determined in each fraction and in the original pooled sample by incubation with cholesterol CHOD-PAP Reagent (Roche, Woerden, The Netherlands). Absorbance was measured at 492 nm.
Plasma cytokines and chemokines were measured using ProcartaPlex™ Multiplex Immunoassays Mouse Cytokine and Chemokine Panel 1 (26 plex), according to manufacturer's protocol (eBioscience, San Diego, CA, USA) and read on a Luminex Magpix (Luminex Corporation, Austin, Tx, USA).

Histology and morphometry
Paraffin sections (5 µm thick) were routinely stained with HPS (hematoxylin-phloxine-saffron), which were used to determine plaque size. Picrosirius red staining was used to visualize collagen and for measurement of necrotic core size. Plaque composition was further examined by staining for smooth muscle cells (alpha smooth muscle actin, Sigma) and macrophages (MAC 3, BD-Pharmingen, San Diego, CA, USA). The amount of mast cells and their activation status was visualized using an enzymatic staining kit (Naphtol-CAE, Sigma).
Morphometric analysis (Leica Qwin image analysis software) was performed on HPS-stained atherosclerotic lesions at site of maximal stenosis. (Immuno) histochemical stainings were quantified by computer assisted analysis (Leica, Qwin, Cambridge, UK) and expressed as the percentage of positive stained area of the total lesion area. Mast cells were counted manually. A mast cell was considered resting when all granula were maintained inside the cell, while mast cells were assessed as activated when granula were deposited in the tissue surrounding the mast cell. The necrotic core was defined as the a-cellular, debris-rich plaque area as percentage of total plaque area.

Cell culture
Bone marrow (BM) cells isolated from C57Bl/6 mice were cultured in petridishes (Greiner Bio-one, Alphen aan den Rijn, Netherlands) for 7 days in RPMI medium supplemented with 20% fetal calf serum (FCS), 2 mmol/L l-glutamine, 100 U/mL penicillin and 100 µg/mL streptomycin and 30% L929 cell-conditioned medium, as the source of macrophage colony-stimulating factor (M-CSF), to generate BM-derived macrophages (BMDMs)[10]. For generation of primary mast cells, BM cells were cultured in RPMI medium supplemented with 10% IL-3 supernatant (supernatant of WEHI-cells overexpressing and secreting murine Interleukin 3 (mIL3)), 1 mM sodium pyruvate, MEM non-essential amino acids, 10% FCS, 2 mmol/L l-glutamine, 100 U/mL penicillin and 100 µg/mL streptomycin for 4 weeks[11]. Mast cell purity and maturation was determined microscopically by staining of cytospins with 0.5% aqueous toluidin blue. Primary cultured murine smooth muscle cells (vSMC) and cell lines for fibroblasts (3T3) and endothelial cells (H5V) were cultured in complete DMEM medium supplemented with 10% FCS, 2 mmol/L l-glutamine, 100 U/mL penicillin and 100 µg/mL streptomycin in T75 tissue culture flasks (Greiner Bio-one).
Mast cells, fibroblasts, smooth muscle cells and endothelial cells were plated in triplicate at a density of 10^6 cells/mL. GSOs were added overnight at a concentration of 5 µg/mL, after which the cells were lysed for RNA isolation.
For BMDMs, GSOs were added immediately after isolation from BM in a concentration of 5 µg/mL. After three days medium was refreshed with a similar addition of GSOs in a concentration of 5 µg/mL. Four days later, medium was removed and cells were lysed for RNA isolation.

RNA isolation, cDNA synthesis and qPCR
Three carotid artery segments from 7 days after collar placement were pooled and homogenized by grounding using a Pellet Pestle Cordless Motor (Kimble Chase Life Science, USA). Spleen, liver and intestines from these mice were isolated and homogenized by grounding with the use of liquid nitrogen. Also, BM was isolated, after which total RNA was extracted using a standard TRIzol-chloroform protocol. RNA concentration, purity and integrity were examined by nanodrop (Nanodrop® Technologies). MiR quantification was performed according to manufacturer's protocol using TaqMan® miR assays (Applied Biosystems, Foster City, CA, USA). qPCRs were run on a 7900HT Fast Real-Time PCR System (Applied Biosystems). Normalization of data was performed using a stably expressed endogenous control (mmu-let-7c; for the liver miR-122 was used).
For the in vitro experiments, total RNA was extracted from the cells using the guanidine thiocyanate (GTC) method[12]. RNA was reverse transcribed by M-MuLV reverse transcriptase (RevertAid, MBI Fermentas, Leon-Roth, Germany) and used for quantitative analysis of mouse genes (Supplemental Table 3) with an ABI PRISM 7700 Taqman apparatus (Applied Biosystems). Murine HPRT and RPL27 were used as standard housekeeping genes.

Cholesterol efflux assay
BMDMs, cultured and treated with GSOs as described above, were seeded at a density of $0.5*10^6$ per well. The next day, medium was aspirated and cells were loaded with 20 mg/mL cholesterol for 24 hours with 1 µCi/mL 3H-cholesterol in DMEM with 10% BSA, with the addition of either GSO-control or GSO-494 (5 µg/mL) (n=6). The following day, loading medium was removed and the cells were washed with PBS, after which DMEM/10%BSA was added to the cells for one hour. Subsequently, the medium was removed and cells were incubated overnight with control DMEM/10%BSA medium or DMEM/10%BSA medium supplemented with HDL (50 µg/mL). After a 24-hour efflux period, radioactivity in the cells and medium was determined by liquid scintillation counting (Packard 1500 Tricarb, Downers Grove, IL, USA). Cholesterol efflux is defined as ($dpm_{medium}/dpm_{cells}+dpm_{medium}$) x100%, and is depicted as the percentage HDL specific efflux, which was corrected for non-specific efflux to control medium.

Collagen synthesis assay
To measure collagen production by vSMC, cells were seeded at a density of 0.2*106 cells per well. After attachment of the cells,

control medium or medium containing GSO-control or GSO-494 (5 µg/mL), was added. Subsequently, 1 µCi [^{3}H]proline (Perkin Elmer, Groningen, The Netherlands) in the presence of 50 µg/mL ascorbic acid was added and incubated overnight at 37°C. Cells were detached from the wells in 20 mM Tris*HCl/0.36 mM CaCl2 (pH=7.6) and sonicated for 2 minutes. Collagen was degraded by incubation with 100 U/mL collagenase for 2 hours at 37°C, after which samples were centrifuged for 15 minutes at 13.2 g. Proteins were precipitated for 30 minutes on ice using 50% trichloroacetic acid, after which [^{3}H]proline content in the supernatant as a measure for collagen production was quantified in a liquid scintillation analyzer as described above. Protein content was measured using a standard BCA protein assay.

Statistical analysis

Data are expressed as mean ± SEM. Two-tailed Student's t-tests were used to compare individual groups in the in vivo studies. Non-parametric data were analyzed using a Mann-Whitney U test. A level of $P<0.05$ was considered significant.

References

1. Seo D, Wang T, Dressman H, et al. Gene expression phenotypes of atherosclerosis. *Arterioscler Thromb Vasc Biol*. 2004;24:1922-1927.
2. Tabibiazar R, Wagner RA, Ashley EA, et al. Signature patterns of gene expression in mouse atherosclerosis and their correlation to human coronary disease. *Physiol Genomics*. 2005;22:213-226.
3. Fu S, Zhao H, Shi J, et al. Peripheral arterial occlusive disease: global gene expression analyses suggest a major role for immune and inflammatory responses. *BMC Genomics*. 2008;9:369.
4. Laukkanen J, Ylä-Herttuala S. Genes involved in atherosclerosis. *Exp Nephrol.* 2002;10:150-163.
5. Lusis AJ. Genetics of atherosclerosis. *Trends Genet*. 2012;28:267-275.
6. Von der Thüsen JH, van Berkel TJC, Biessen EAL. Induction of rapid atherogenesis by perivascular carotid collar placement in apolipoprotein E-deficient and low-density lipoprotein receptor-deficient mice. *Circulation*. 2001;103:1164-1170.
7. Welten SM, Bastiaansen AJ, de Jong R, et al. Inhibition of 14q32 MicroRNAs miR-329, miR-487b, miR-494 and miR-495 Increases Neovascularization and Blood Flow Recovery after Ischemia. *Circ Res*. 2014;115:696-708.
8. Nossent AY, Eskildsen TV, Andersen LB, et al. The 14q32 MicroRNA-487b Targets the Antiapoptotic Insulin Receptor Substrate 1 in Hypertension-Induced Remodeling of the Aorta. *Ann Surg*. 2013;258:743-753.
9. Bhagat L, Putta MR, Wang D, et al. Novel oligonucleotides containing two 3'-ends complementary to target mRNA show optimal gene-silencing activity. *J Med Chem*. 2011;54:3027-3036.
10. Zhao Y, Pennings M, Hildebrand RB, et al. Enhanced foam cell formation, atherosclerotic lesion development, and inflammation by combined deletion of ABCA1 and SR-BI in Bone marrow-derived cells in LDL receptor knockout mice on western-type diet. *Circ Res*. 2010;107:e20-e31.
11. Razin E, Marx G. Thrombin-induced degranulation of cultured bone marrow-derived mast cells. *J Immunol*. 1984;133:3282-3285.
12. McGookin R. RNA extraction by the guanidine thiocyanate procedure. *Methods Mol Biol*. 1985;2:113-116.

Supplemental Figures and Tables

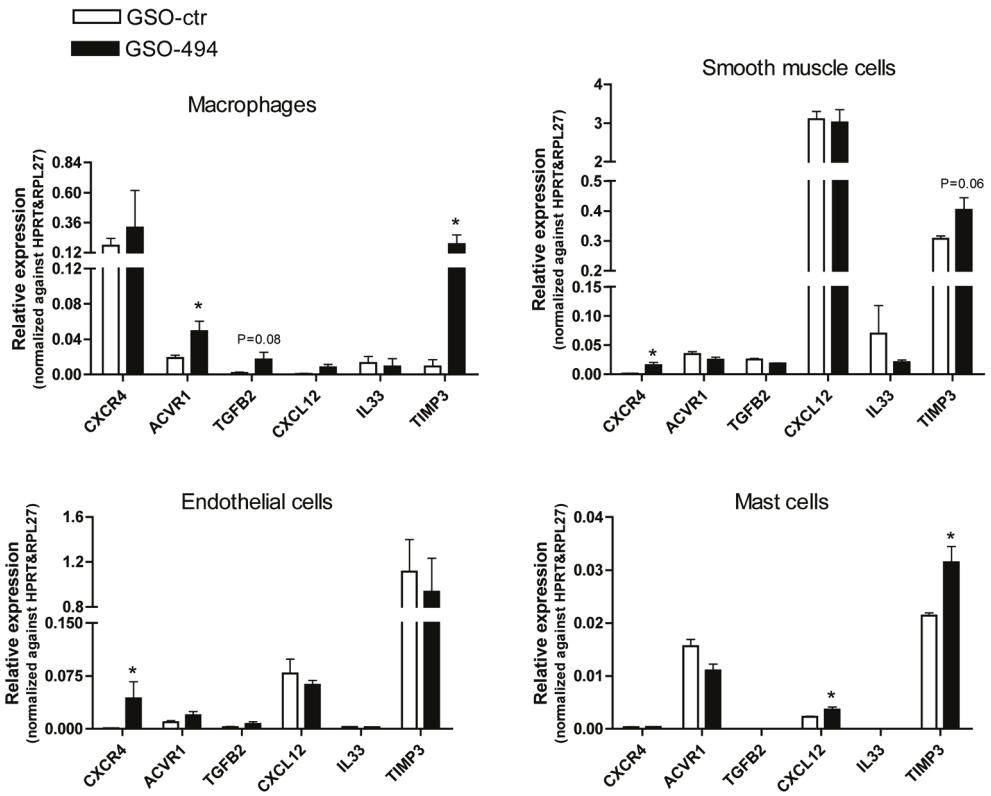

Supplemental Figure 1. In vitro expression of selected target genes CXCR4, ACVR1, TGFB2, CXCL12, IL33 and TIMP3 in macrophages, smooth muscle cells, endothelial cells, and mast cells after treatment with either GSO-494 or GSO-ctr, relative to expression of HPRT & RPL27. *P<0.05, compared to GSO-ctr.

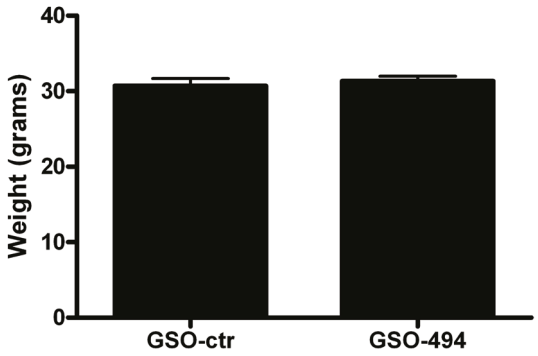

Supplemental Figure 2. Body weight (in grams) of mice after treatment with GSO-494 or GSO-ctr.

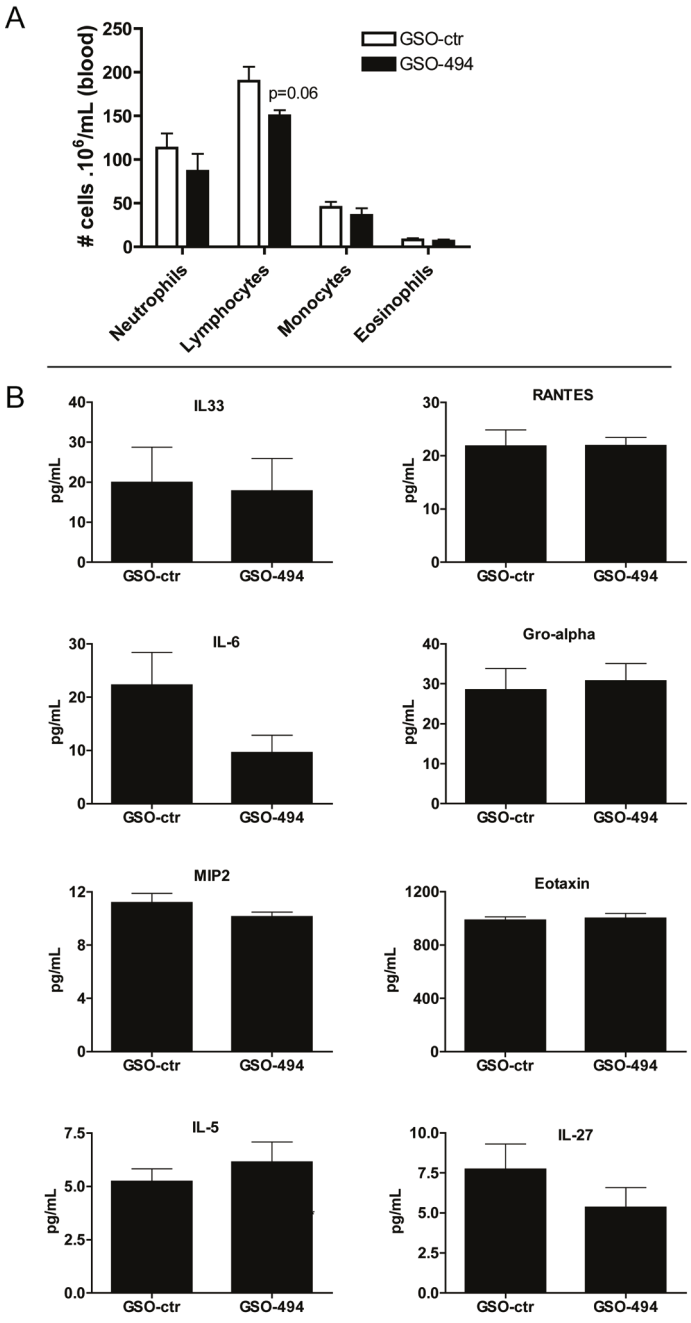

Supplemental Figure 3. A trend towards a decrease in absolute amount of lymphocytes 4 days after treatment with GSO-494 was observed, while the absolute numbers of neutrophils, monocyte or eosinophils remained unaltered compared to GSO-ctr. (A) Multiplex immunoassay analysis showed no major changes in systemic cytokine and chemokine levels after GSO-494 treatment (B).

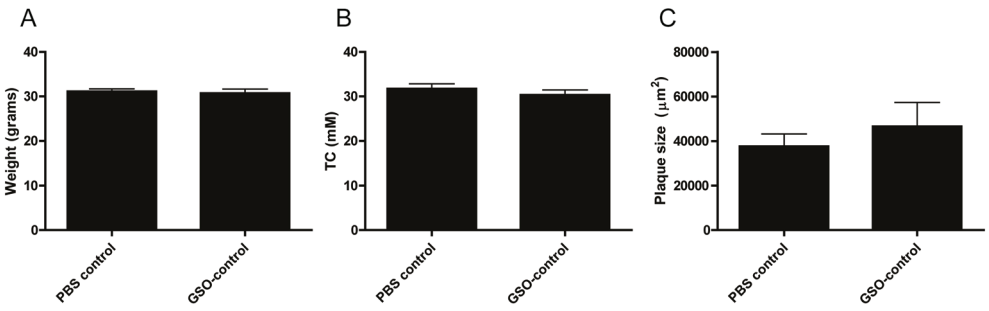

Supplemental Figure 4. (A) Body weight (in grams), (B) plasma cholesterol and (C) plaque size of mice treated with PBS or GSO-ctr.

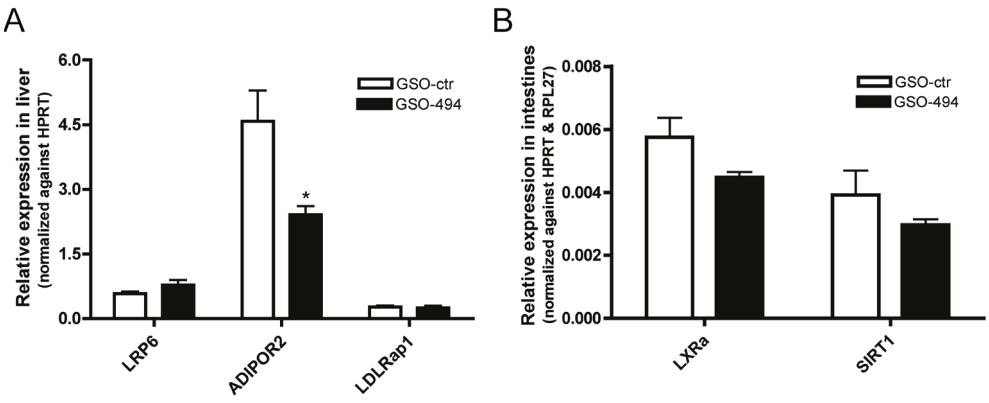

Supplemental Figure 5. (A) Expression of selected target genes LRP6, ADIPOR2 and LDLRap1 in the liver and (B) LXRa and SIRT1 in the intestines at 3 days after GSO injection, normalized against HPRT and RPL27. *P<0.05, compared to GSO-ctr.

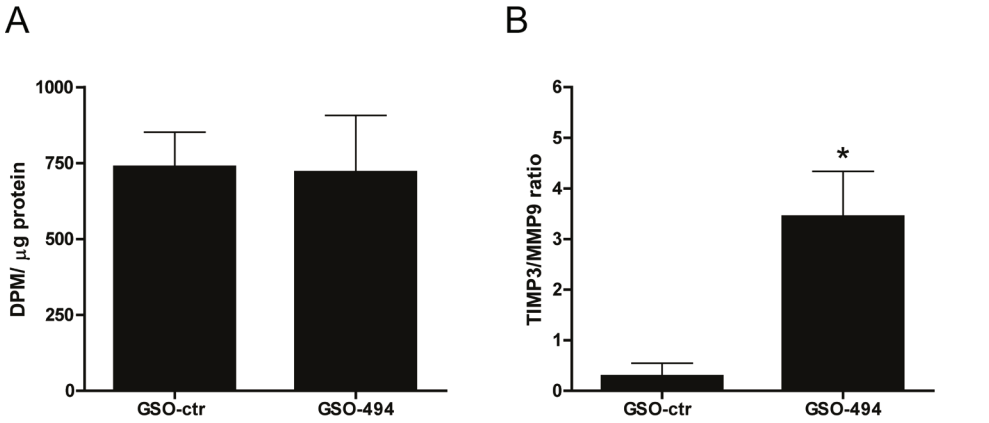

Supplemental Figure 6. (A) Collagen synthesis of smooth muscle cells treated with GSO-494 and (B) TIMP3/MMP9 ratio in macrophages was increased after GSO-494 treatment as TIMP3 expression significantly increased, whereas MMP9 expression remained unaltered. *P<0.05, compared to GSO-ctr.

MiR	# of putative target genes
miR-590-3p	65
miR-129-5p/129ab-5p	46
miR-186	46
***miR-495/1192**	45
*miR-543	45
miR-24/24ab/24-3p	45
miR-150/5127	44
miR-340-5p	43
miR-203	42
*miR-410/344de/344b-1-3p	42
miR-326/330/330-5p	41
*miR-300/381/539-3p	41
miR-128/128ab	41
miR-149	40
miR-33ab/33-5p	40
miR-181abcd/4262	39
*miR-539/539-5p	39
***miR-494**	38
*miR-485-5p/1698/1703/1962	38
*miR-376c/741-5p	37
miR-204/204b/211	37
miR-290-5p/292-5p/371-5p/293	37
miR-384/384-3p	37
miR-93/93a/105/106a/291a3p/294/295/302abcde /372/373/428 /519a/520be/520acd-3p/1378/1420ac	36
miR-197	36
*miR-544/544ab/544-3p	36
miR-23abc/23b-3p	35
miR-124/124ab/506	35
miR-185/882/3473/4306/4644	35
miR-874	34
miR-374ab	34
miR-17/17-5p/20ab/20b-5p/93/106ab/427/518a-3p/519d	33
miR-320abcd/4429	33
miR-214/761/3619-5p	33
*miR-134/3118	32
miR-488	32
miR-339b/339-5p/3586-5p	31
miR-15abc/16/16abc/195/322/424/497/1907	31
***miR-329/329ab/362-3p**	30
miR-873	30
miR-155	30
miR-125a-5p/125b-5p/351/670/4319	30
miR-9/9ab	29
miR-199ab-5p	29
miR-27abc/27a-3p	29
miR-342-3p	29
miR-34ac/34bc-5p/449abc/449c-5p	29
miR-141/200a	28
miR-103a/107/107ab	28
miR-7/7ab	28

Supplemental table 1A. Reversed target prediction performed by analyzing binding sites in human target genes. MiRs of the 14q32 miR gene cluster are identified with an asterisk (*).

MiR	# of putative target genes
miR-466l-3p	63
miR-694	44
miR-325-3p	43
miR-340-5p	42
miR-875-3p.m	42
*miR-410/344de/344b-1-3p	41
miR-1958	40
miR-335-3p	40
miR-5101	40
miR-677/4276	40
miR-590-3p	39
miR-692/4753-3p	39
***miR-495/1192**	37
miR-326/330/330-5p	37
miR-466k/466di-5p	37
miR-181abcd/4262	37
miR-186	36
miR-669f-3p	35
***miR-494**	34
*miR-300/381/539-3p	34
miR-450b-3p/3100-5p	34
miR-141/200a	34
miR-452-3p	34
miR-5110	34
miR-5113	34
miR-669m-3p	34
miR-1587/3083/4505	33
miR-1756b/1896	33
miR-33ab/33-5p	33
miR-545/3065/3065-5p	33
miR-125b-2-3p	32
miR-1941-5p	32
miR-207	32
miR-290-5p/292-5p/371-5p/293	32
miR-3057-3p	32
miR-3474	32
miR-466d/466l-5p	32
miR-488	32
miR-5112	32
*miR-543	32
miR-683	32
miR-712	32
miR-1968	31
miR-214/761/3619-5p	31
miR-297b-3p/466ade-3p/467g	31
miR-3090/4726-3p	31
miR-873	31
*miR-377	30
miR-204/204b/211	30
*miR-1906	30

Supplemental table 1B. Reversed target prediction performed by analyzing binding sites in murine target genes. MiRs of the 14q32 miR gene cluster are identified with an asterisk (*).

MiR	Sequence
mmu-miR-494	5’-UGAAACAUACACGGGAAACCUC-3’
mmu-miR-495	5’-AAACAAACAUGGUGCACUUCUU-3’
mmu-miR-329	5’-AACACACCCAGCUAACCUUUUU-3’
mmu-miR-122	5’-UGGAGUGUGACAAUGGUGUUUG-3’
mmu/hsa-miR-let7c-5p	5’-UGAGGUAGUAGGUUGUAUGGUU-3’
GSO	**Sequence**
mmu-GSO-494	3’-ACTTTGTATGTGCCCTTTGGAG-X-GAGGTTTCCCGTGTATGTTTCA-3’
negative control GSO	3’-TGTACGACTCCATAACGGT-X-TGGCAATACCTCAGCATGT-3’

Supplemental table 2. The sequences of miRs and GSOs used for in vitro and in vivo experiments are listed.

Gene	Forward primer	Reversed primer
CXCR4	GGTGATCCTGGTCATGGGTT	TGACAGGTGCAGCCGGTA
TIMP3	ACTGTGCAACTTTGTGGAGAGGT	GAGACACTCATTCTTGGAGGTCA
CXCL12	TGCATCAGTGACGGTAAACCA	GGCTCTCGAAGAACCGGC
ADIPOR2	CATGTTTGCCACCCCTCAGTATC	AGCCAGCCTATCTGCCCTATG
TGFB2	AGACCCCACATCTCCTGCTAATC	AATCAATGTAAAGAGGGCGAAGGC
LRP6	TTTGAACCCACCACCATCGCCTGCC	GCGGTGCAAAGTGCCGGTAGCTGTA
LDLrap1	CAGCCTCACTAGCCAGCTCATC	CGAACACCTTGTCGTGCATCTTG
LXRa	TCAGCATCTTCTCTGCAGACC	TCATTAGCATCCGTGGGAACA
SIRT1	ACCTTGGAGCAGGTTGCAGGAATCCAA	GCACCTAGGGCACCGAGGAACTACC
ACVR1	GGAAGTCCGCCATTGCCCATC	GGTTGTTTCCCACATCAAGCTGGT
IL33	CCAGGTGCTACTACGCTACTATGAG	AGATGTCTGTGTCTTTGATGGGACT
HPRT	TTGCTCGAGATGTCATGAAGGA	AGCAGGTCAGCAAAGAACTTATAG
RPL27	TGAAAGGTTAGCGGAAGTGC	TTTCATGAACTTGCCCATCTC

Supplemental table 3. List of all primers used for in vitro and in vivo experiments.